Supporting Information for:

Catenanes from Catenanes: Quantitative Assessment of Cooperativity in Dynamic Combinatorial Catenation

Jianwei Li, Piotr Nowak, Hugo Fanlo-Virgos, Sijbren Otto*

Centre for Systems Chemistry, Stratingh Institute, University of Groningen, Nijenborgh 4, 9747 AG Groningen, The Netherlands

Email: s.otto@rug.nl

Table of Contents

1. Materials

All chemicals, unless otherwise stated, were purchased from Sigma-Aldrich and used as received. HPLC or LC-MS grade solvents were obtained from BIOSOLVE. All solvents used in synthesis were distilled prior to use and anhydrous solvents were distilled from a drying agent under a nitrogen atmosphere.

2. Synthesis of building block 1

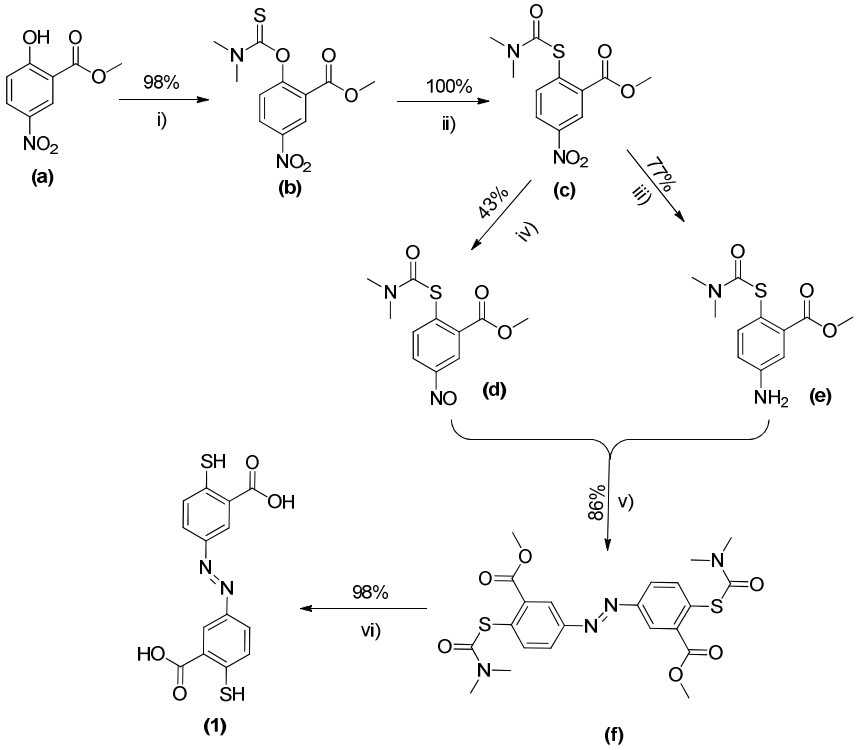

Scheme S1. Building block synthesis route. i) Me_2N-C(S)-Cl, DABCO, 0°C→RT, DMF; ii) 150°C, 20 min; iii) Zn, acetic acid, 120°C, 45 min; iv) 2-methoxyethanol, water, NH_4Cl, Zn, $FeCl_3$, 5h; v) acetic acid, RT, overnight; vi) 1.75 M KOH in diethyleneglycol, 30 min, 110°C.

Synthesis of methyl 2-((dimethylcarbamothioyl)oxy)-5-nitrobenzoate (b)

Methyl 2-hydroxy-5-nitrobenzoate (**a**) (2.00 g, 10.0 mmol) was dissolved in anhydrous DMF (20.0 mL) at room temperature under a nitrogen atmosphere. Dimethylthiocarbamoyl chloride (1.85 g, 15.0 mmol) was added, followed by gradual addition of DABCO (1.68 g, 15.0 mmol), turning the solution orange. The reaction mixture was stirred for 24 hours, until TLC analysis indicated complete consumption of starting materials. A mixture of brine and water (400 mL, 50:50 composition) was added, causing a large amount of precipitate to form. After a further 10 minutes of stirring, the precipitate was filtered, washed with distilled water, and dried, yielding a white solid (2.80 g, 98%). ^{1}H NMR (400 MHz, $CDCl_3$) δ ppm 8.84 (d,

J = 2.82 Hz, 1H), 8.39 (dd, *J* = 8.87, 2.83 Hz, 1H), 7.29 (d, *J* = 8.87 Hz, 1H), 3.89 (s, 3H), 3.45 (br s, 3H), 3.41 (br s, 3H). ^{13}C NMR (100 MHz, $CDCl_3$) δ (ppm): 186.0, 162.8, 158.0, 145.0, 128.0, 127.1, 126.4, 125.3, 52.7, 43.4, 39.1. ESI-HRMS $[M+H]^+$ found: 285.0552 (expected: 285.0540).

Synthesis of methyl 2-((dimethylcarbamoyl)thio)-5-nitrobenzoate (c)

Methyl 2-((dimethylcarbamothioyl)oxy)-5-nitrobenzoate (**b**) (0.500 g, 2.00 mmol) was heated in at 150 °C for 20 minutes, forming a brown liquid. The reaction mixture was cooled down to room temperature and solidified. The solid was ground to give a yellow power (0.500 g, 100%). ^{1}H NMR (400 MHz, $CDCl_3$) δ ppm 8.53 (d, *J* = 2.1 Hz, 1H), 7.91 (d, *J* = 8.4 Hz, 1H), 7.81 (d, *J* = 8.4 Hz, 1H), 3.97 (s, 4H), 3.11 (br s, 6H). ^{13}C NMR (100 MHz, $CDCl_3$) δ (ppm): 165.1, 164.2, 147.1, 139.0, 137.4, 135.0, 125.4, 125.2, 53.6, 52.4, 37.2. ESI-HRMS: $(M+H)^+$ found: 285.0552 (expected: 285.0540).

Synthesis of methyl 2-((dimethylcarbamoyl)thio)-5-nitrosobenzoate (d)[16]

Methyl 2-((dimethylcarbamoyl)thio)-5-nitrobenzoate (**c**) (11.4 g, 80.0 mmol) was dissolved in methoxyethanol (400 mL) and a solution of NH_4Cl (6.79 g, 127 mmol) in H_2O (100 mL) was added. The reaction mixture was warmed to 30°C and finely powdered zinc (20.4 g, 312 mmol) was added in portions over a period of 30 minutes maintaining the temperature between 30-35°C while stirring vigorously. The mixture was allowed to react at 35°C for 2 hours and then filtered and washed with methoxyethanol. The filtrate was added to a solution of $FeCl_3$ (25.2 g, 155 mmol) in H_2O (300 mL) and ethanol (120 mL) over the course of 90 minutes while the temperature was kept at -5°C. After 1 hour, the mixture was poured into water (800 mL) and the yellow precipitate collected and purified by silica column chromatography (hexane/ethyl acetate 3/1) yielding **d** as a light green solid (43%). ^{1}H NMR (400 MHz, $CDCl_3$) δ ppm 8.71 (d, *J* = 2.57 Hz, 1H), 8.26 (dd, *J* = 8.66, 2.59 Hz, 1H), 7.83 (d, *J* = 8.65 Hz, 1H), 3.93 (s, 3H), 3.14 (br s, 3H), 3.03 (br s, 3H). ^{13}C NMR (100 MHz, $CDCl_3$) δ (ppm): 189.1, 174.6, 152.1, 138.4, 136.7, 135.3, 124.8, 125.1, 53.2, 51.9, 36.7. ESI-HRMS: $(M+H)^+$ found: 268.0474 (expected: 268.0481).

Synthesis of methyl 5-amino-2-((dimethylcarbamoyl)thio)benzoate (e)

Methyl 2-((dimethylcarbamoyl)thio)-5-nitrobenzoate (**c**) (5.00 g, 35.0 mmol) was dissolved in acetic acid (200 mL), and heated to 120°C under a nitrogen atmosphere. Zinc powder (50.0 g) was added in portions, and the reaction was left to stir under reflux for 45 minutes. The reaction mixture was filtered and washed with acetic acid, diluted with water (150 mL), and the product extracted into dichloromethane (5 × 50 mL). The organic layer was then washed with sodium hydroxide (10%, aqueous solution) until the aqueous layer remained basic, then washed once more with water. The organic layer was dried with Na_2SO_4, filtered, and concentrated in *vacuo*, to yield a yellow viscous oil. Diethyl ether (5.00 mL) was added, causing a white solid to precipitate overnight. The crude product was recrystallized by dissolving in a minimum amount of dichloromethane, followed by addition of diethyl ether, and evaporating at room temperature, yielding a white solid (3.50 g, 77%). ^{1}H NMR (400 MHz, $CDCl_3$) δ ppm 7.33 (d, *J* = 8.34 Hz, 1H), 7.17 (d, *J* = 2.68 Hz, 1H), 6.77 (dd, *J* = 8.34, 2.70 Hz, 1H), 3.84 (s, 3H), 3.04 (s, 6H). ^{13}C NMR (100 MHz, $CDCl_3$) δ (ppm): 167.7, 167.3, 147.8, 139.2, 136.5, 117.6, 116.7, 115.9, 52.1, 37.0. ESI-HRMS: $(M+H)^+$ found: 255.0798 (expected: 255.0798).

Synthesis of (E)-dimethyl 5,5'-(diazene-1,2-diyl)bis(2-((dimethylcarbamoyl)thio) benzoate) (f)

Methyl 2-((dimethylcarbamoyl)thio)-5-nitrosobenzoate (**d**) (2.68 g, 10.0 mmol) and methyl 5-amino-2-((dimethylcarbamoyl)thio)benzoate (**e**) (2.54 g, 10.0 mmol) were mixed in acetic acid (40 ml) and stirred at room temperature overnight in the dark. An orange percipitate formed and was collected by filtration as final product, yielding 4.33 g, 86%. ^{1}H NMR (400 MHz, $CDCl_3$) δ ppm 8.45 (d, *J* = 2.2 Hz, 2H), 8.03 (dd, *J* = 8.4, 2.2 Hz, 2H), 7.79 (d, *J* = 8.3 Hz, 2H), 3.94 (s, 6H), 3.10 (s, 12H). ^{13}C NMR (100 MHz, $CDCl_3$) δ (ppm): 166.4, 165.5, 151.7, 139.2, 137.8, 135.3, 133.7, 125.9, 125.1, 52.5, 37.1. ESI-HRMS: $(M+H)^+$ found: 505.1141 (expected: 505.1137).

Synthesis of (E)-5,5'-(diazene-1,2-diyl)bis(2-mercaptobenzoic acid) (1)

Under a nitrogen atmosphere, (E)-dimethyl 5,5'-(diazene-1,2-diyl)bis(2-((dimethyl carbamoyl)thio)benzoate) (**f**) (0.50 g, 1.0 mmol) was suspended in a 1.75 M solution (10.0 mL) of KOH in diethyleneglycol that had been purged with nitrogen for 2 hours. The solution was heated at 110°C for 30 minutes. After the solution had cooled down to room temperature, 80 mL of purged water was added followed by rapid addition of 10% HCl (6.00 mL). The precipitate was fitered quickly to avoid oxidation, washed extensively with purged water and dried under vacuum overnight to give orange building block **1** (0.32g, 98%). ^{1}H NMR (400 MHz, $(CH_3)_2CO$) δ ppm 8.68 (d, *J* = 2.2 Hz, 2H), 7.99 (dd, *J* = 8.5, 2.3 Hz, 2H), 7.72 (d, *J* = 8.5 Hz, 2H), 4.17-4.12 (m, 2H). ^{13}C NMR could not be recorded due to poor solubility and limited stability. ESI-HRMS: $(M-H)^-$ found: 333.0005 (expected: 333.0004).

3. Identification of library members

Analytical HPLC Analysis

Analytic HPLC was carried out on Hewlett Packard 1050 or 1100 systems coupled to UV detectors and the data were processed using HP Chemstation software. Separations were performed on a reversed phase Zorbax C8 column (4.6 x 150 mm, 5 µm particle size, Agilent). Except where otherwise stated, the chromatography was carried out at 45 °C and using UV detection at 254 nm. We recorded the UV spectrum of all the catenanes. They showed the same absorbance (Figure S12). The following LC analysis method was used:

Time (min)	B%
0	5
30	95

Solvent A: Water (0.1% v/v formic acid); Solvent B: Acetonitrile (0.1% v/v formic acid)

Flow rate: 1.0 mL/min

LC-MS Analysis

An Accela High Speed LC system (ThermoFisher Scientifics, Courtaboeuf, France) was coupled to a LTQ-Fleet Ion Trap Mass Spectrometer. Water was obtained from a MilliQ Gradient system and LC-MS-grade acetonitrile was bought from BIOSOLVE.

Analysis of samples was performed using a reversed-phase HPLC column (Zorbax C8, 4.6 x 150 mm, 5 µm, Agilent) at 45 °C with an injection volume of 4 µL. All UV traces were obtained by monitoring at 254 nm. The LC-MS analysis method is the same as the HPLC method described above.

Mass spectra were recorded in positive ion mode. The electrospray voltage was set to 4.20 kV, and the capillary voltage was set to 25.0 V; the sheath and auxiliary gas flows (both nitrogen) were 5.00 L/min and 5.00 L/min, respectively, and the drying gas temperature was 320 °C.

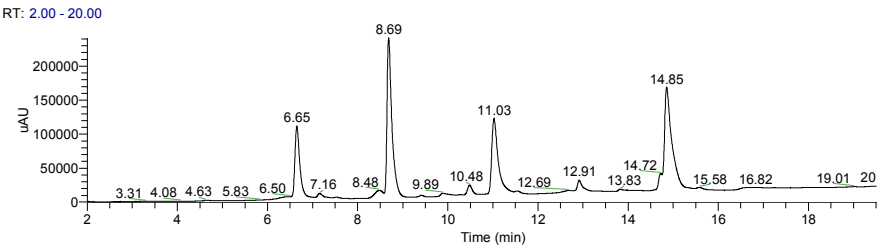

Figure S1. HPLC analysis of the fully oxidized library made from building blocks **1** (2.0 mM) and β-CD (0.50 mM) in a 0.50 mL borate buffer (50 mM, pH 8.3).

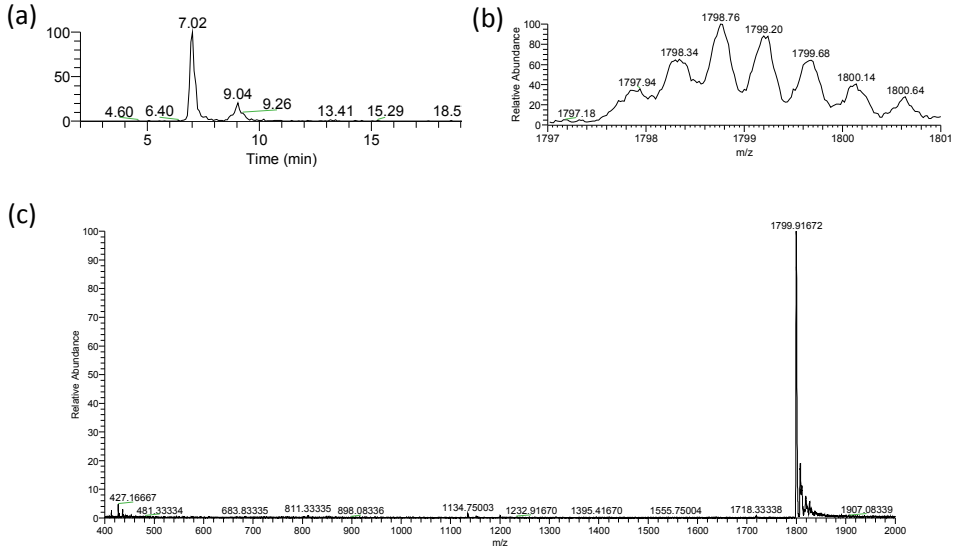

Figure S2. (a) Extracted ion chromatogram of m/z = 1799.50 - 1800.50 corresponding to **4**-2β-CD; (b) isotopic profile of the peak observed at 1799; (c) ESI-MS spectrum of the HPLC peak at 6.65 min. Expected m/z for [**4**-2β-CD+2H]$^{2+}$=1799.8453.

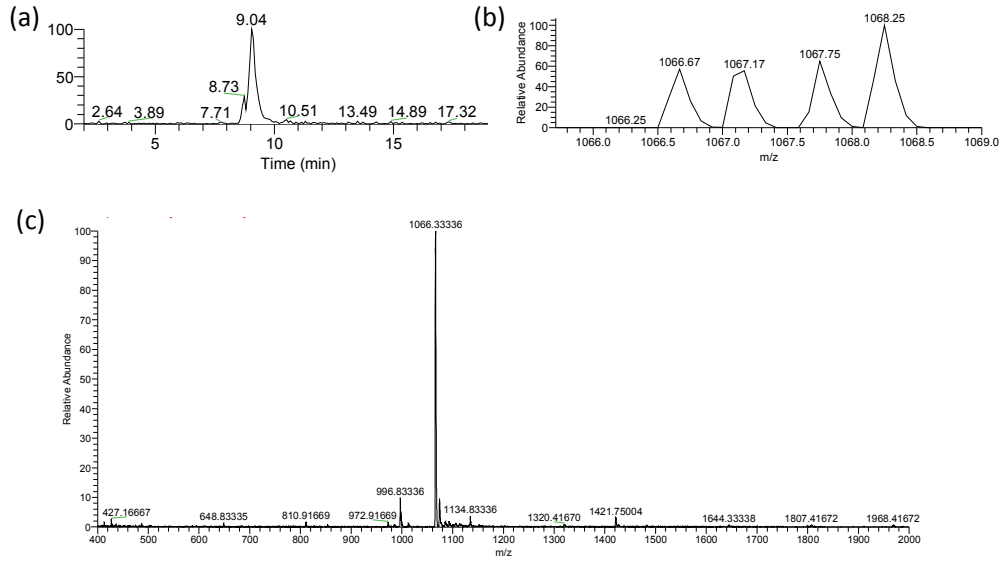

Figure S3. (a) Extracted ion chromatogram of m/z = 1065.50 - 1066.50 corresponding to of **3**-β-CD; (b) isotopic profile of the peak observed at 1066.00; (c) ESI-MS spectrum of the HPLC peak at 8.69 min. Expected m/z for [**3**-β-CD+2H]$^{2+}$=1066.5814.

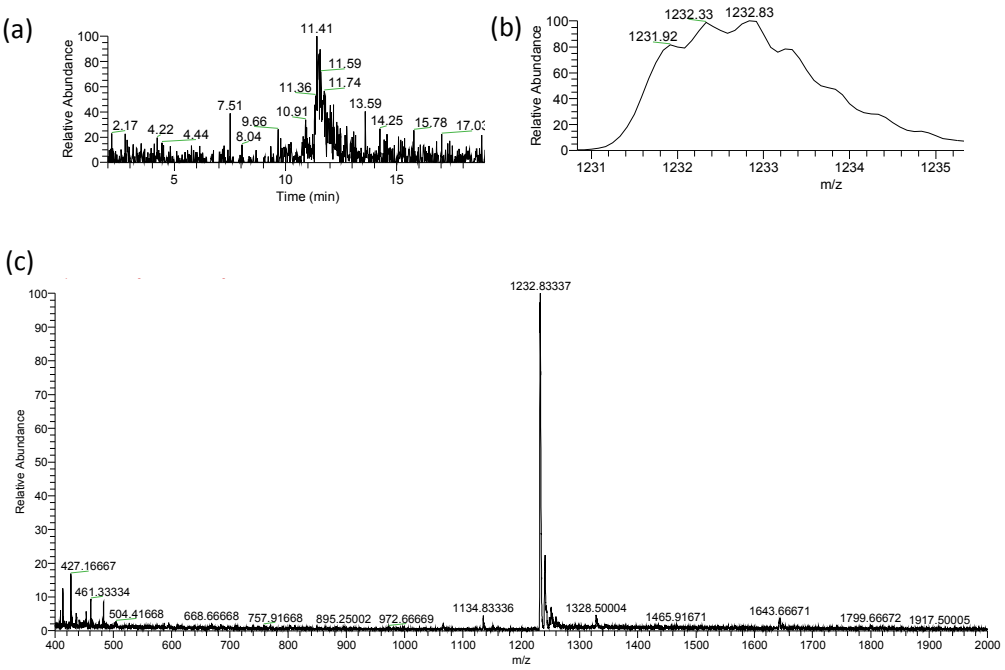

Figure S4. (a) Extracted ion chromatogram of m/z= 1232.00 - 1233.00 corresponding to **4**-β-CD; (b) isotopic profile of the peak observed at 1232.83; (c) ESI-MS spectrum of the HPLC peak at 11.03 min. Expected m/z for [**4**-β-CD+2H]$^{2+}$=1232.8132.

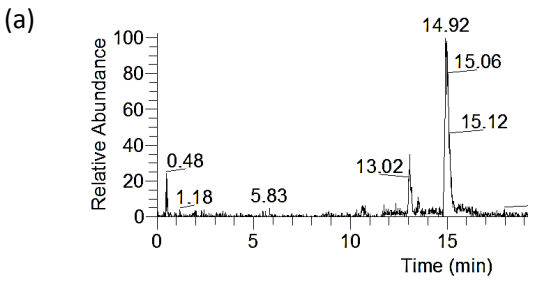

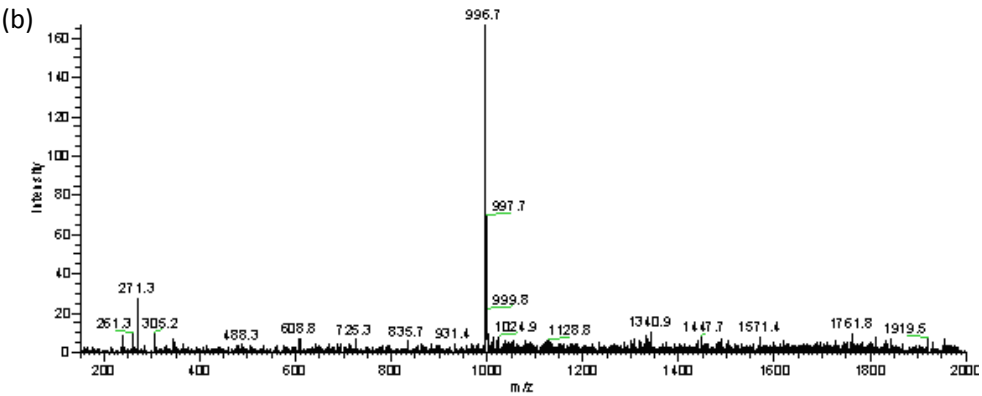

(c)

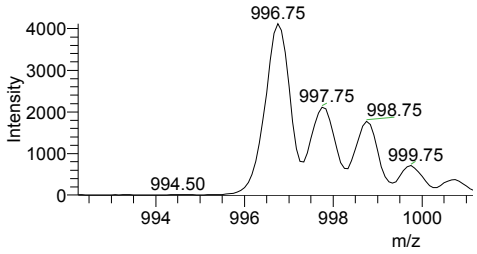

(d)

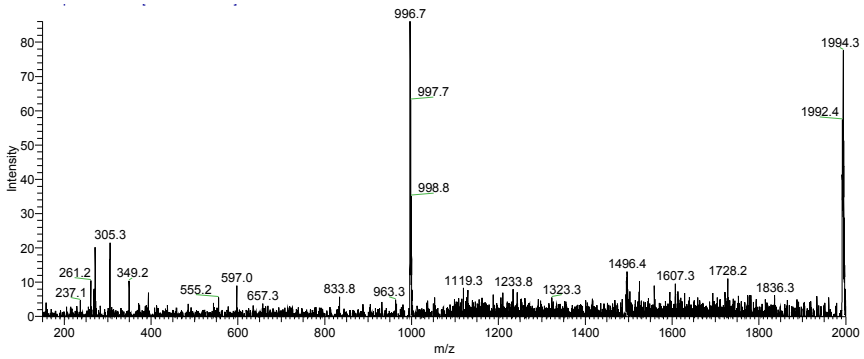

(e)

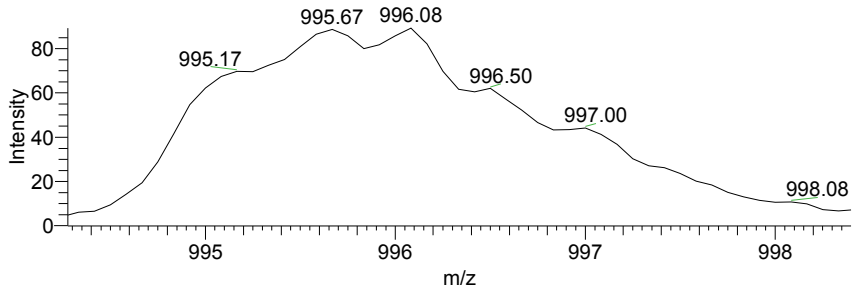

Figure S5. (a) Extracted ion chromatogram of m/z= 996.50 - 997.50 corresponding to singly charge **2** and doubly charge **3**. Two peaks corresponding to HPLC peaks at 12.91 min and 14.85 min were found; (b) ESI-MS spectrum of the HPLC peak at 12.91 min. and (c) isotopic profile of the peak observed at 996.75 in (b). Expected m/z for $[\mathbf{3}+H]^{+}$=996.91. The mass of the HPLC peak at 12.91 min corresponds to that of **3.** (d) ESI-MS spectrum of the HPLC peak at 14.85 min and (e) isotopic profile of the peak observed at 996.75 in (d). Expected m/z for $[\mathbf{2}+H]^{2+}$=996.91.

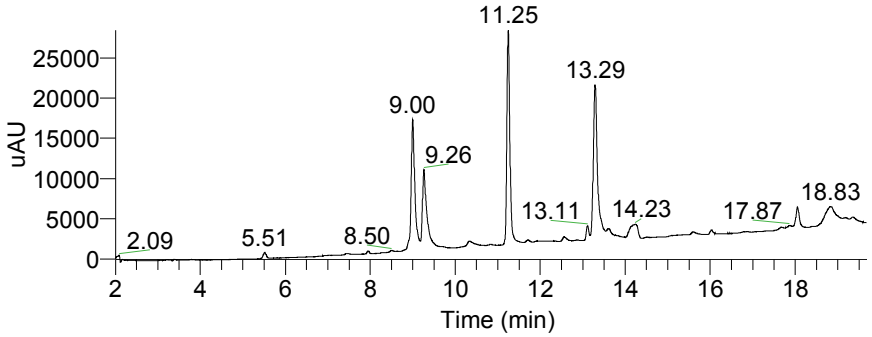

Figure S6. HPLC analysis of the fully oxidized library made from building blocks **1** (2.0 mM) and γ-CD (4 mM) in a 0.5 mL borate buffer (50 mM, pH 8.3).

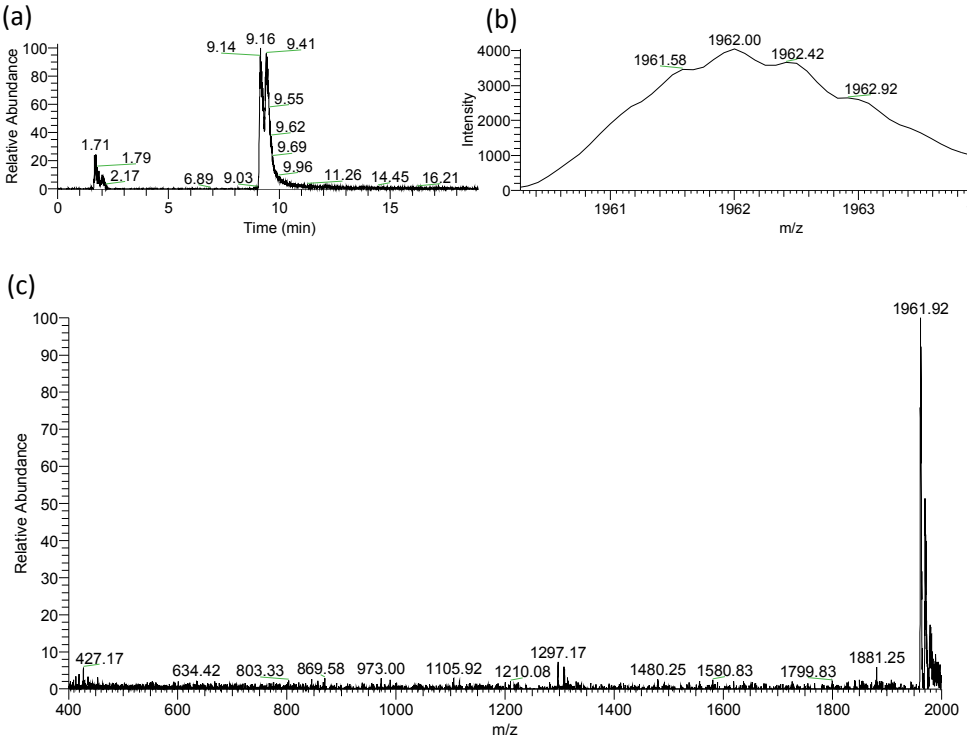

Figure S7. (a) Extracted ion chromatogram of m/z = 1961.50 - 1962.50 corresponding to **4**-2γ-CD; (b) isotopic profile of the peak observed at 1961.92; (c) ESI-MS spectrum of the HPLC peak at 9.00 min and 9.26 min. Expected m/z for $[\mathbf{4}\text{-}2\gamma\text{-CD}+2H]^{2+}$=1962.04.

(a)

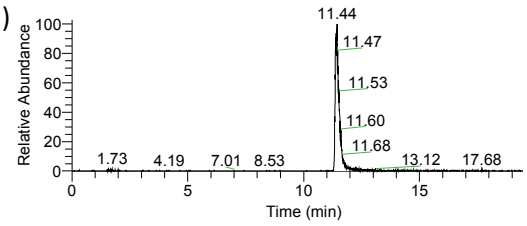

(b)

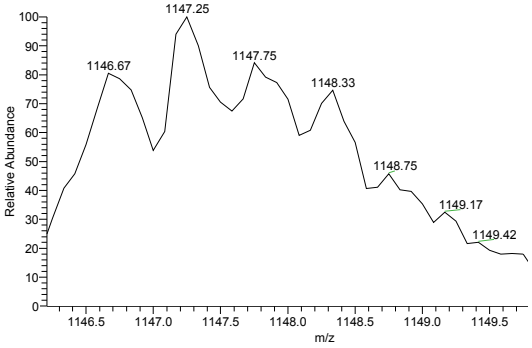

(c)

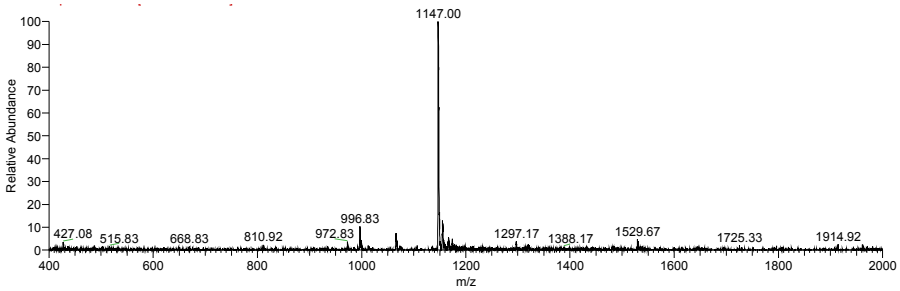

Figure S8. (a) Extracted ion chromatogram of m/z = 1146.50 - 1147.50 corresponding to **3**-γ-CD. (b) isotopic profile of the peak observed at 1147.00; (c) ESI-MS spectrum of the HPLC peak at 11.25 min. Expected m/z for $[\mathbf{3}\text{-γ-CD+2H}]^{2+}$=1147.13.

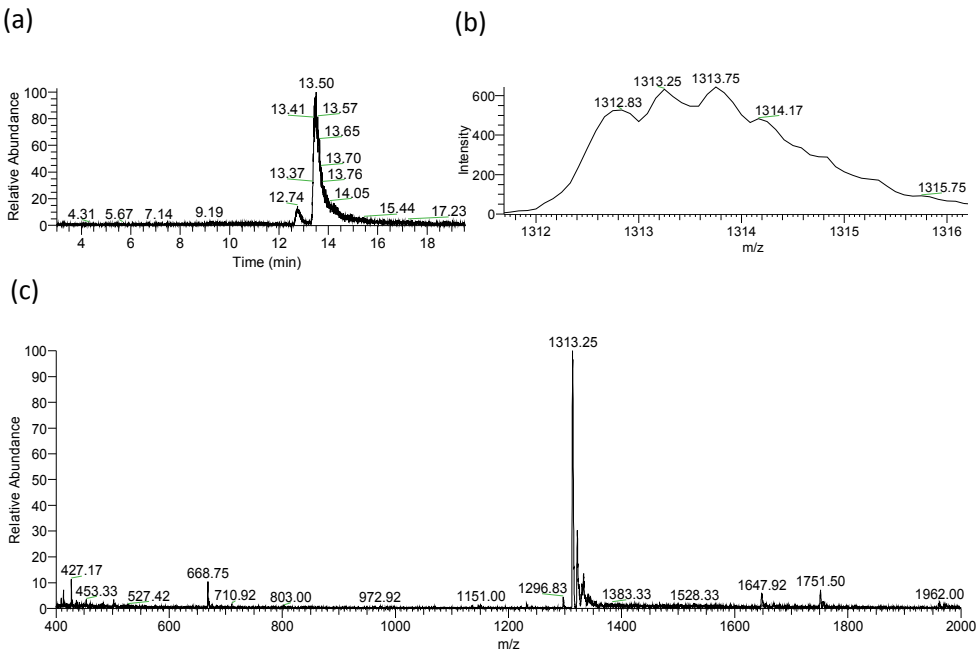

Figure S9. (a) Extracted ion chromatogram of m/z = 1312.80 - 1313.80 corresponding to **4**-γ-CD; (b) isotopic profile of the peak observed at 1313.25; (c) ESI-MS spectrum of the HPLC peak at 13.29 min. Expected m/z for [**4**-γ-CD+2H]$^{2+}$=1313.30.

4. ^{1}H-NMR spectra of catenanes

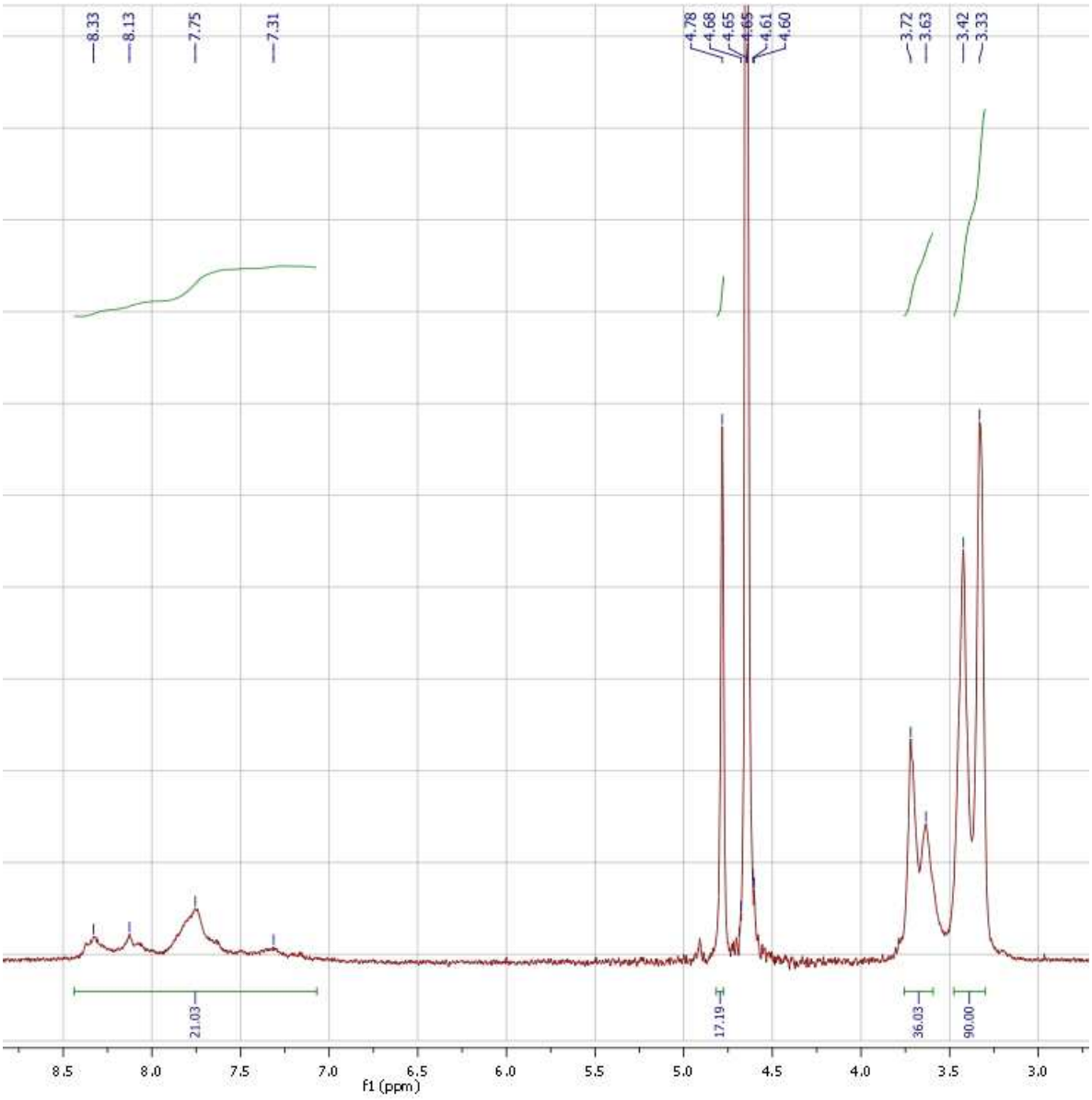

Figure S10. ^{1}H NMR of [3]catenanes **4**-2β-CD (0.3 mM) in D_2O (pD 8.3).

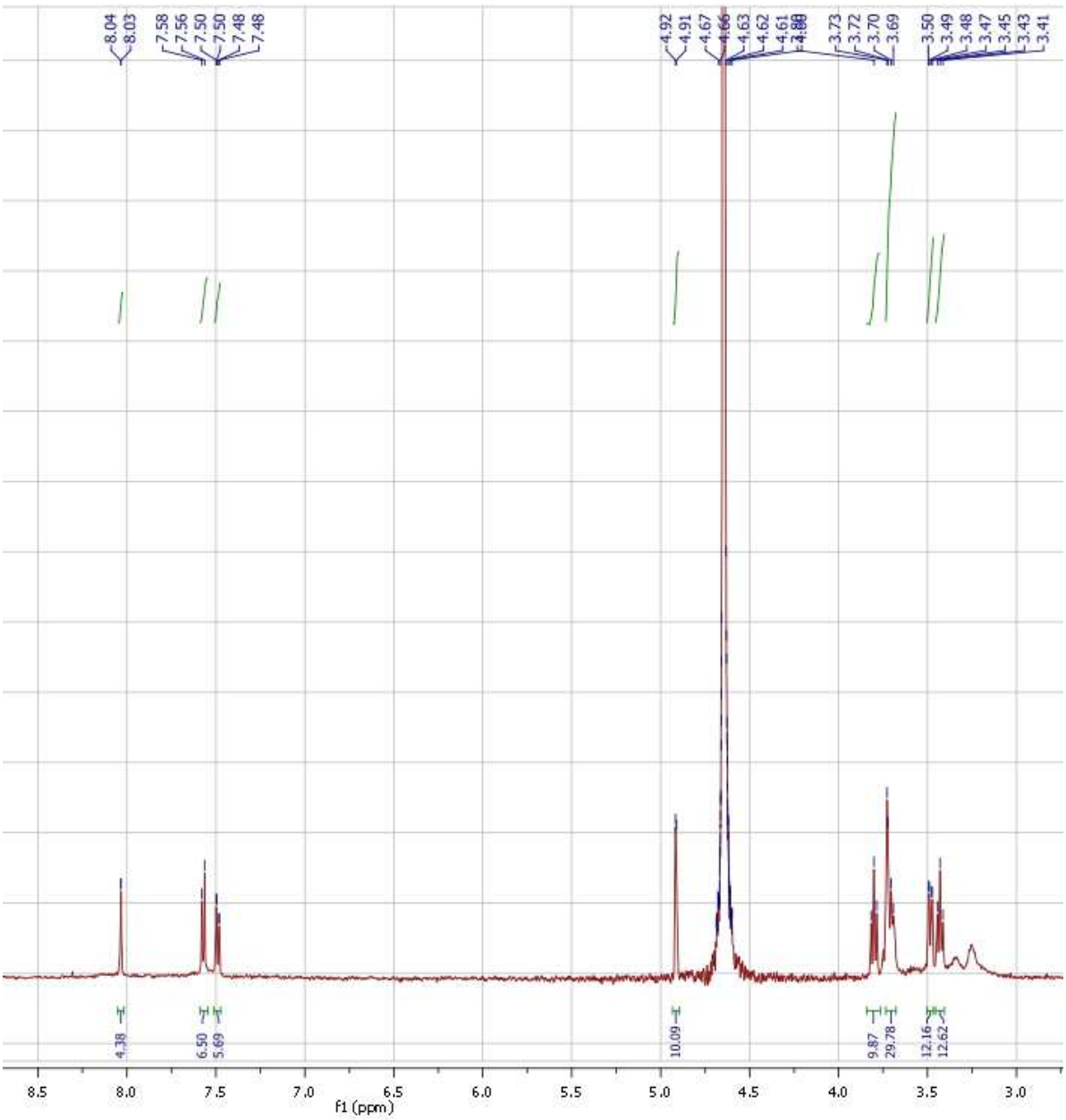

Figure S11. ^{1}H NMR of [2]catenane **3-**β-CD (0.5 mM) in D_2O (pD 8.3).

5. Evaluation of Equilibrium Constants by DCLfit

The procedure of evaluating equilibrium constants by DCLfit starts by defining a proper model containing the various host-guest binding equilibrium, which has been explained in the main text (See Scheme 2). In order to obtain accurate estimates of the equilibrium constants in the system, it is necessary to accumulate a data set for a number of different DCLs under a range of experimental conditions (i.e. different building block and cyclodextrin concentrations). Thus two series of eight DCLs were set up, with concentrations of building block **1** (2.0 mM) and β-CD or γ-CD in the range of 0 and 5 mM respectively. When all the libraries were fully oxidized and equilibrated, the concentrations of DCL members in the DCLs with or without β-CD or γ-CD were determined by analytical HPLC. The peak areas of species in libraries with various concentration of β-CD or γ-CD are shown in Table S1 and Table S2 respectively.

Table S1. Peak area (mAU × sec.) of species in libraries with different concentration of β-CD

[β-CD] (M)	Area of **4**-2β-CD	Area of **3**-β-CD	Area of **4**-β-CD	Area of **3**	Area of **4**	Area of **2**	Total Peak Area
0	0	0	0	8.03E+02	2.77E+02	2.03E+03	3.11E+03
2.50E-04	1.62E+02	8.96E+02	4.17E+02	2.01E+02	1.32E+02	1.21E+03	3.02E+03
5.00E-04	5.51E+02	1.30E+03	4.32E+02	8.80E+01	5.60E+01	7.45E+02	3.18E+03
1.00E-03	9.93E+02	1.60E+03	2.25E+02	5.40E+01	2.30E+01	4.21E+02	3.31E+03
1.25E-03	1.08E+03	1.57E+03	2.18E+02	4.10E+01	1.60E+01	3.00E+02	3.22E+03
3.00E-03	1.51E+03	1.29E+03	1.44E+02	1.60E+01	9.00E+00	1.13E+02	3.09E+03
4.00E-03	1.64E+03	1.27E+03	5.00E+01	1.80E+01	1.00E+01	7.60E+01	3.06E+03
5.00E-03	1.72E+03	1.30E+03	3.10E+01	3.40E+01	3.00E+00	1.10E+02	3.20E+03
Average Value of Peak Area							3.15E+03

Table S2. Peak area (mAU × sec.) of species in libraries with different concentration of γ-CD

[γ-CD] (M)	Area of **4**-2γ-CD	Area of **3**-γ-CD	Area of **4**-γ-CD	Area of **3**	Area of **4**	Area of **2**	Total Peak Area
0	0	0	0	8.71E+02	2.35E+02	1.94E+03	3.05E+03
2.50E-04	6.00E+00	4.94E+02	1.03E+03	1.36E+02	1.19E+02	1.60E+03	3.39E+03
7.50E-04	1.44E+02	7.13E+02	1.44E+03	5.30E+01	5.00E+01	6.89E+02	3.09E+03
1.00E-03	2.36E+02	8.52E+02	1.57E+03	4.60E+01	4.60E+01	5.75E+02	3.32E+03
1.25E-03	2.92E+02	8.95E+02	1.63E+03	3.90E+01	3.90E+01	4.63E+02	3.36E+03
1.50E-03	3.88E+02	9.12E+02	1.56E+03	3.90E+01	3.80E+01	3.61E+02	3.30E+03
2.00E-03	5.44E+02	9.76E+02	1.51E+03	3.70E+01	3.40E+01	2.92E+02	3.40E+03
3.00E-03	8.57E+02	9.79E+02	1.32E+03	3.50E+01	2.70E+01	1.76E+02	3.39E+03
4.00E-03	1.08E+03	9.65E+02	1.14E+03	3.50E+01	2.10E+01	9.60E+01	3.34E+03
5.00E-03	1.15E+03	9.47E+02	1.05E+03	5.50E+01	3.60E+01	8.60E+01	3.29E+03
Average Value of Peak Area							3.29E+03

We recorded the UV spectra of each catenane library member. The normalized UV spectra of the catenanes are essentially identical (Figure S12). From HPLC analysis using UV detection at 254 nm, we found that the total HPLC peak area is similar and independent of the library composition. The peak area of each library species is listed above in Table S1 and Table S2. These data demonstrate that the various library members have similar molar absorbtivities per unit of building block **1**.

$$[\text{library member}] = \frac{\text{peak area of library member}}{\text{average total peak area} \times \text{number of units of } \mathbf{1}} \times 2\ \text{mM} \qquad \text{[equation S1]}$$

We calculated the concentration of each library species using equation S1. The concentrations of all the library members are listed in Table S3 and S4.

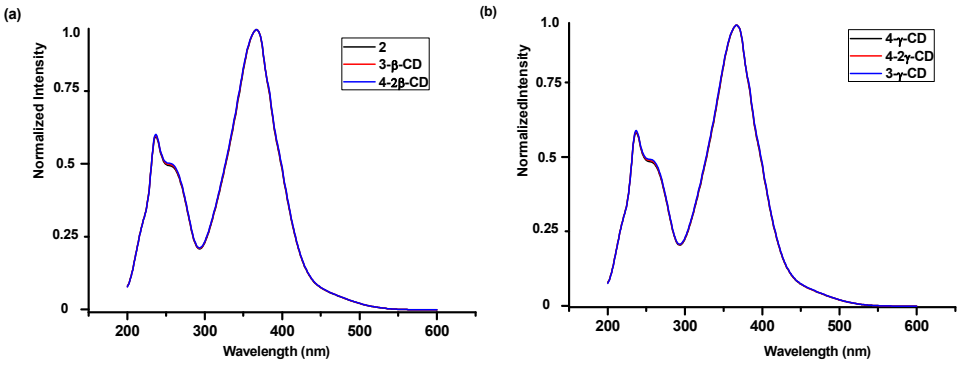

Figure S12. Normalized UV spectra (highest absorbance = 1) of (a) catenane **2** and catenanes formed from β-CD and (b) γ-CD. The fact that the UV spectra in each graph overlap indicates that catenation does not affect the UV spectra of the macrocycles involved.

Table S3. Concentration (M) of species in libraries with different concentration of β-CD

[β-CD]	[**4**-2β-CD]obs	[**3**-β-CD]obs	[**4**-β-CD]obs	[**3**]obs	[**4**]obs	[**2**]obs
0	0	0	0	1.63E-04	4.21E-05	2.06E-04
2.50E-04	2.46E-05	1.82E-04	6.34E-05	4.07E-05	2.01E-05	1.23E-04
5.00E-04	8.39E-05	2.65E-04	6.58E-05	1.79E-05	8.51E-06	7.56E-05
1.00E-03	1.51E-04	3.24E-04	3.42E-05	1.10E-05	3.48E-06	4.27E-05
1.25E-03	1.64E-04	3.18E-04	3.32E-05	8.30E-06	2.39E-06	3.04E-05
3.00E-03	2.30E-04	2.62E-04	2.20E-05	3.30E-06	1.44E-06	1.15E-05
4.00E-03	2.49E-04	2.58E-04	7.60E-06	3.58E-06	1.52E-06	7.66E-06
5.00E-03	2.62E-04	2.64E-04	4.65E-06	6.98E-06	5.32E-07	1.12E-05

Table S4. Concentration (M) of species in libraries with different concentration of γ-CD

[γ-CD]	[**4**-2γ-CD]obs	[**3**-γ-CD]obs	[**4**-γ-CD]obs	[**3**]obs	[**4**]obs	[**2**]obs
0	0	0	0	1.80E-04	3.64E-05	2.00E-04
2.50E-04	1.00E-06	1.02E-04	1.60E-04	2.81E-05	1.84E-05	1.65E-04
7.50E-04	2.23E-05	1.47E-04	2.24E-04	1.10E-05	7.80E-06	7.11E-05
1.00E-03	3.66E-05	1.76E-04	2.43E-04	9.54E-06	7.08E-06	5.94E-05
1.25E-03	4.53E-05	1.85E-04	2.52E-04	8.02E-06	6.08E-06	4.77E-05
1.50E-03	6.01E-05	1.88E-04	2.42E-04	8.00E-06	5.93E-06	3.73E-05
2.00E-03	8.43E-05	2.02E-04	2.34E-04	7.54E-06	5.31E-06	3.02E-05
3.00E-03	1.33E-04	2.02E-04	2.04E-04	7.18E-06	4.20E-06	1.82E-05
4.00E-03	1.68E-04	1.99E-04	1.76E-04	7.17E-06	3.33E-06	9.86E-06
5.00E-03	1.78E-04	1.96E-04	1.62E-04	1.14E-05	5.64E-06	8.89E-06

After calculating the concentrations, we used the DCLFit program to fit the binding constants using the model shown in Scheme 2 in the main text. The program first guesses the binding constants and then minimizes the error between the observed (Tables S3 and S4) and calculated library distributions. We used the ordinary least squares error method, Nelder-Mead Simplex minimizer, and repeated the

procedure 500 times use the Monte-Carlo approach to ensure that the global error minimum was found. The lowest error results (shown in Table 1 of the main text) were found 496 and 498 times for β-CD and γ-CD, respectively. Since γ-CD has a relatively big cavity, we also envisioned a possibility of inclusion complexes between the CD and either collapsed **4** or even **4**-γ-CD. Fitting results based on equilibria involving such noncatenative template effects remained almost unchanged; i.e. inclusion binding constants were at least two orders of magnitude lower than for catenative binding, therefore we did not include include inclusion complexes in the model. The comparisons between fitted concentration profiles and observed profiles are shown below.

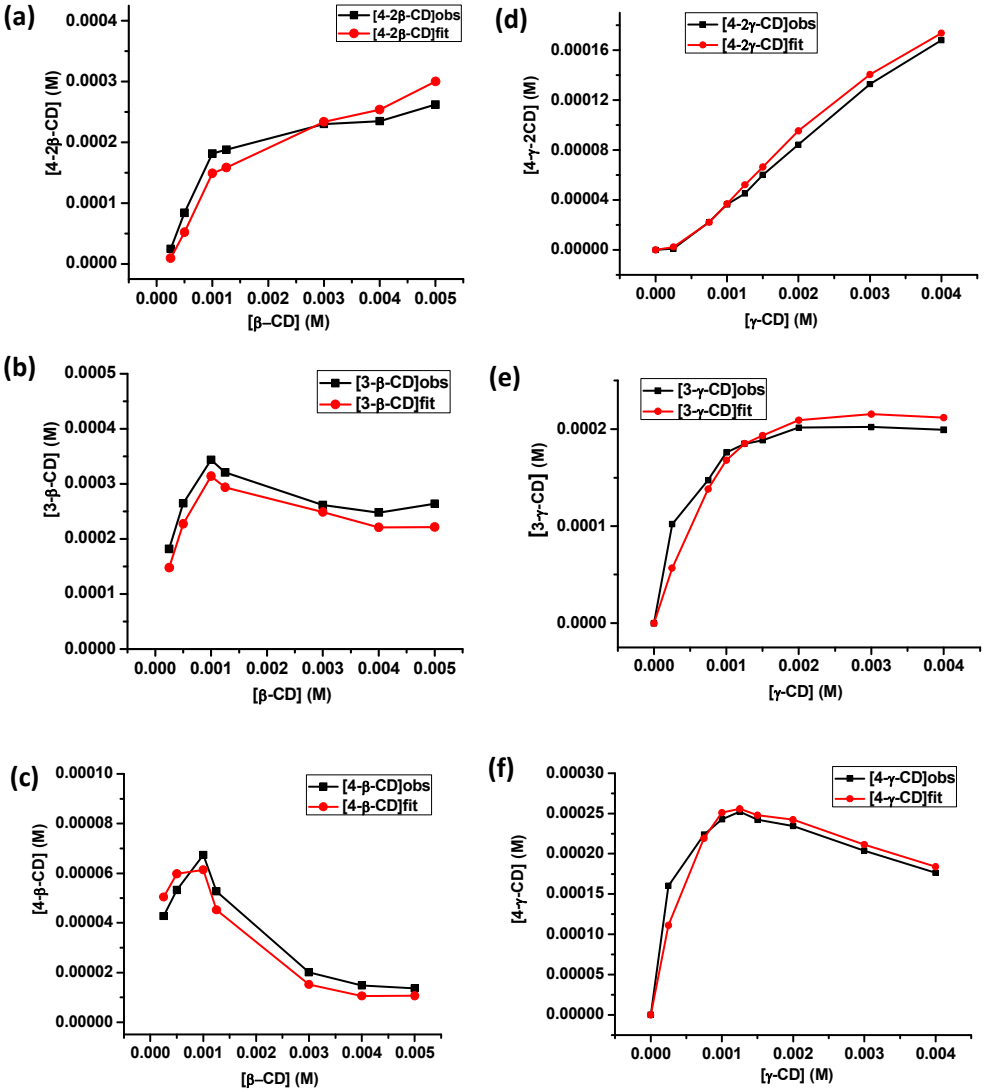

Figure S13. Observed and fitted concentrations of (a) **4**-2β-CD; (b) **3**-β-CD; (c) **4**-β-CD as a function of the concentration of the β-CD template; (d) **4**-2γ-CD; (e) **3**-γ-CD; (f) **4**-γ-CD as a function of the concentration of the γ-CD template.

6. UV-vis titrations of 1 to β-CD and γ-CD

UV-vis measurements were performed using a Varian Cary Bio UV-visible spectrophotometer at 298 ± 0.1 K. A quartz cuvette with 1 cm path length was used for the measurements. The absorption spectra were recorded from 200 nm to 650 nm.

We determined the equilibrium constant for binding of building block **1** to β-CD and γ-CD by UV titration. The concentration of building block **1** was kept at 2.5×10^{-5} M. Upon the addition of β-CD, the absorbance at 475 nm decreased, accompanied by an increasing absorbance at 255 nm (Figure S14a). We attribute the fact that the UV spectrum of **1** changes upon complexation, while the UV spectra of the catenanes and the uncatenated azobenzene macrocycles are very similar, to changes in the thiol protonation state upon binding to the cyclodextrins.

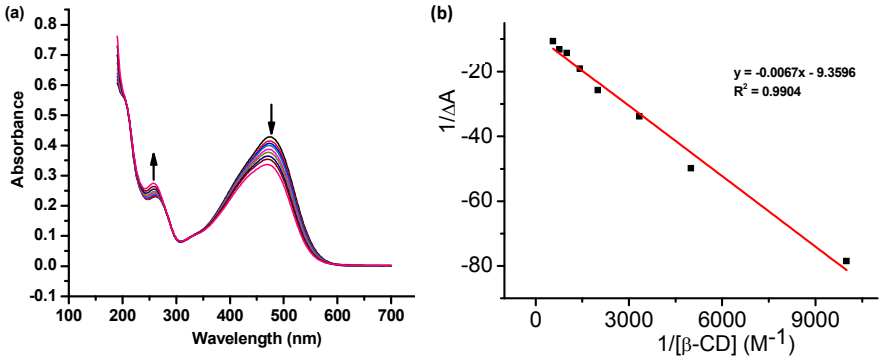

Figure S14. (a) Changes in UV absorbance of building block **1** upon the addition of β-CD. The concentration of building block **1** is 2.5×10^{-5} M and the β-CD concentration ranges from 0 to 18 mM ; (b) Hildebrand-Benesi plot of the data of Figure S14a at 475 nm.

We assumed that the stoichiometry of binding between building block **1** and β-CD is 1:1 and fitted our data according to the modified Hildebrand-Benesi equation[1,2]:

$$\frac{1}{\Delta A}=\frac{1}{K_a\Delta\varepsilon[H][G]}+\frac{1}{\Delta\varepsilon[H]} \qquad \text{[equation S2]}$$

[H] and [G] represent the concentration of buiding block **1** (host) and β-CD (guest) respectively. K_a stands for the equilibrium constant for binding of building block **1** to β-CD. ΔA represents the difference of UV absorbance after and before the addition of β-CD. Δε, represents the difference of the molar extinction coefficient between the host and host-guest complex at the wavelength of 475 nm, and is estimated to be 4.27×10^{3} M^{-1} cm^{-1}. The affinity constant was calculated using equation S3:

$$K_a=\frac{1}{k\Delta\varepsilon[H]} \qquad \text{[equation S3]}$$

Where *k* is the slope of the line in Figure S14b.

The equilibrium constant for binding between building block **1** and γ-CD was determined the same way as that for binding of **1** to β-CD (Figure S15).

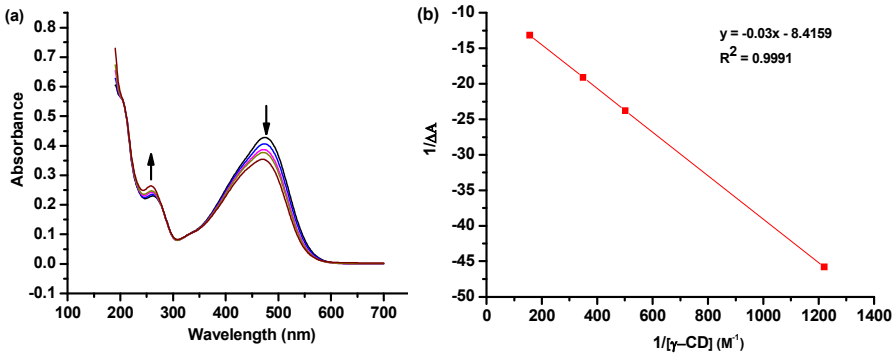

Figure S15. (a) Changes in UV absorbance of the building block **1** upon the addition of γ-CD at 25 ℃; The concentration of building block **1** is 2.5×10^{-5} M in borate buffer (50 mM, pH 8.2) and the γ-CD concentration ranges from 0 to 62 mM ; (b) Hildebrand-Benesi plot of the data of Figure S15a at 475 nm.

7. Molecular dynamics simulations

A. Force field parameters

Cyclodextrin molecules were described using the GLYCAM04 force field[3-5] because of its good description of static and dynamic properties of cyclodextrins[6] and compatibility with the General Amber Force Field (GAFF).[7] Parameters for molecule **4** were taken mainly from GAFF, however its description of the -N=N- bond was poor, leading to spontaneous isomerization between Z and E forms. This problem has been previously spotted and corrected parameters were developed based on the DFT studies.[8] Therefore we have replaced default GAFF parameters for C-N-N-C and N-N-C-C torsional potentials with those proposed by Duchstein *et al.*[8]

B. Charge derivation

The partial atomic charges for molecule **4** were calculated using restrained electrostatic potential fit (RESP) with R.E.D. III.5[9] software interfaced with Gaussian 09.[10] First, azobenzene **1** capped with two neutral -SMe groups (Figure 16) was optimized at HF/6-31G* level of theory. Afterwards, a molecular electrostatic potential (MEP) for two conformations with four reorientations each was computed using a Connolly surface and two RESP stages (RESP-A1 model), enforcing zero charge on the -SMe caps.

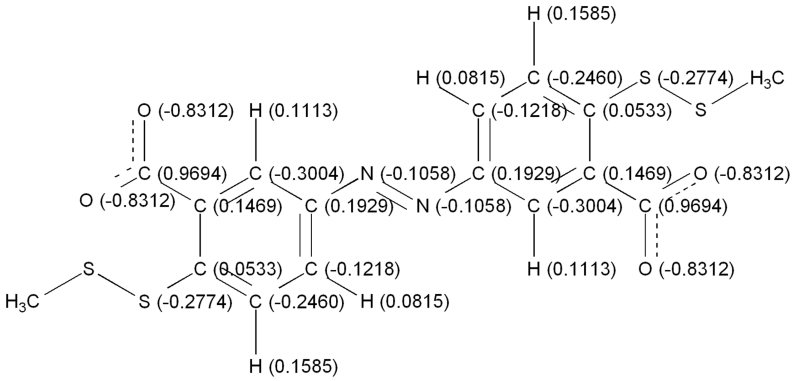

Figure S16. Molecule used for RESP fit.

C. Molecular dynamics simulations

All initial geometries were prepared using Avogadro[11], followed by solvation, topology generation and parameter assignment using leap from the AmberTools 13 package.[12] In all systems containing **4**, the carboxylic groups were fully deprotonated to mimic the experiments which were conducted at pH=8.2. Afterwards, each system was solvated in a truncated octahedral box of TIP3P water[13] with its edges at least 10 Å away from the solute. The negative charge was neutralized by replacing random water molecules with Na^+ cations. After solvation, the systems were minimized with positional restraints on the solute (500 steps of steepest descent and 500 steps of conjugate gradient) and without restraints (1000 steps of steepest descent and 4000 steps of conjugate gradient). Minimization was followed by heating the system to 293 K gradually for 20 ps at constant volume and equilibrating for 100 ps at constant pressure and temperature, monitoring the temperature and density changes to ensure that the

systems were equilibrated properly. After equilibration, the 40 ns simulations were performed (also within an NPT ensemble, at 293 K and 1 atm). To allow 2 fs timesteps, SHAKE[14] was applied to constrain all bonds involving hydrogen. The temperature was controlled using Langevin dynamics[15] with collision frequency of 1.0 ps. The pressure was regulated isotropically to 1.0 bar using Berendsen barostat[16] with relaxation time of 2.0 ps. A nonbonded cutoff was set to 10 Å and long-range electrostatic interactions were computed using particle mesh Ewald.[17] All minimizations and MD were performed using the sander and PMEMD programs from the Amber11 package.[18]

D. Additional MD snapshots

The snapshots shown below were taken from the last analyzed frames of MD simulations performed (40 ns). The stronger binding cyclodextrines (with less hydrophobic surfaces exposed) are drawn in blue and the weaker binding in cyan. Atomic spheres are drawn using Van der Waals radii and the solvent excluded surface area is depicted by the semitransparent gray surface. All images were rendered using VMD[19] and Povray. All structures shown below were deposited to figshare.[20]

Macrocycle **4** has a collapsed conformation for most of the time (structures in Figures S17 and S18), decreasing its water accessible hydrophobic surface. We observed that it can temporarily (between 39.4 and 39.7 ns) open to form a square-shaped conformer shown in Figure S19. We also observed that **4** can assume an open conformation also in **4**-β-CD (Figure S21) for longer periods of time (22.6-26.4 ns). We did not see such behavior in case of **4**-γ-CD. One of the possible explanations for this difference may be the larger size of γ-CD, which allows it to encompass two azobenzene units, preventing them from forming a conformation in which they are perpendicular to each other, while β-CD is generally well localized around only one azobenzene. We did not observe CD changing their azobenzene stations in any of the simulations.

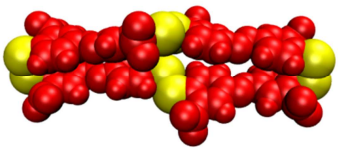

Figure S17. **4** after 29 ns of the simulation.

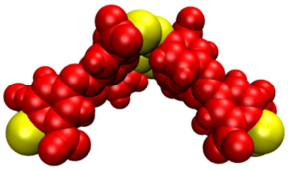

Figure S18. **4** after 35 ns of the simulation.

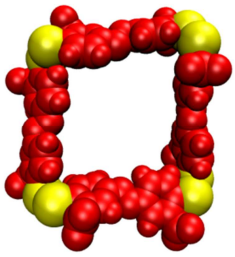

Figure S19. **4** after 39.48 ns of the simulation.

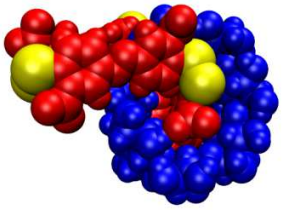

Figure S20. **4**-β-CD after 30 ns of the simulation.

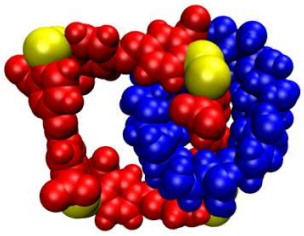

Figure S21. **4**-β-CD after 25 ns of the simulation.

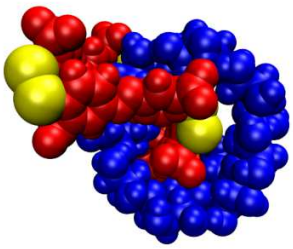

Figure S22. **4**-γ-CD after 30 ns of the simulation.

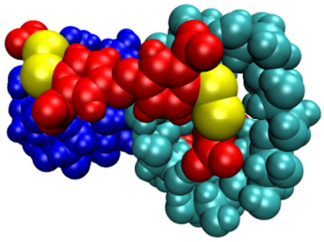

Figure S23. **4**-2β-CD (antiparallel) after 30 ns of the simulation.

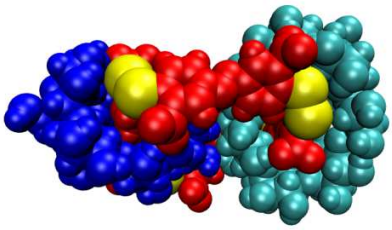

Figure S24. **4**-2β-CD (parallel) after 30 ns of the simulation.

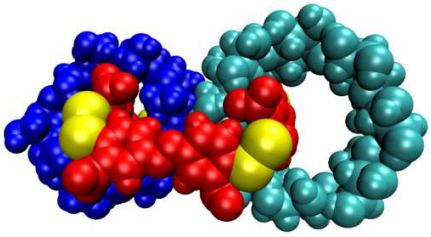

Figure S25. **4**-2γ-CD (antiparallel) after 30 ns of the simulation.

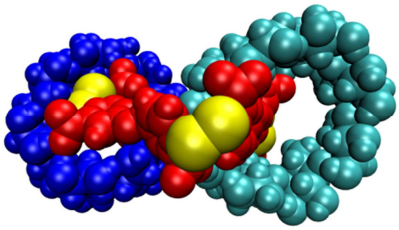

Figure S26. **4**-2γ-CD (parallel) after 30 ns of the simulation.

E. Hydrophobic solvent accessible surface areas (SASAs)

Solvent accessible hydrophobic surface areas were obtained using the cpptraj utility from the AmberTools 13 package.[12] The trajectories were first stripped from water and sodium counterions and then the contributions of the hydrophobic atoms of the azobenzene units and the cyclodextrins were calculated separately. For the cyclodextrin molecules, we considered the hydrogens and oxygens of the hydroxyl groups as hydrophilic, while all other atoms were considered hydrophobic. Since macrocycle **4** contains charged carboxylate groups, water surrounding them is strongly polarized and does not "feel" the hydrophobicity of neighboring hydrophobic groups.[21,22] Therefore we counted the contribution of aromatic carbon which is attached the COO^- group and the two neighboring CH groups as hydrophilic. However, the choice of SASA partitioning between hydrophobic and hydrophilic parts does not influence the relative values in a significant way. All raw data plotted in the following sections were deposited to figshare.[20]

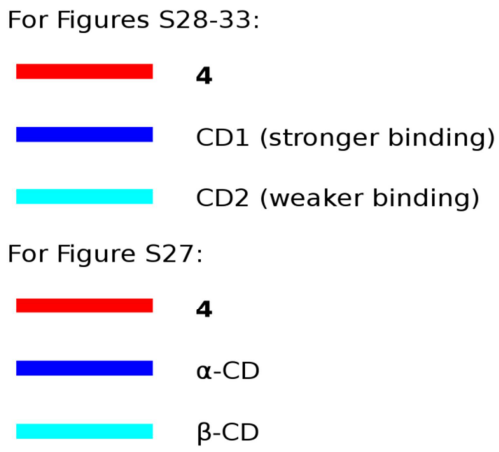

Legend for figures S27-33.

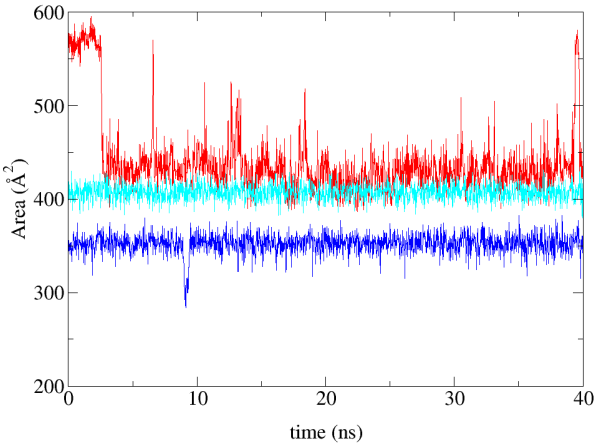

Figure S27. SASA of free substrates: **4**, β-CD, γ-CD.

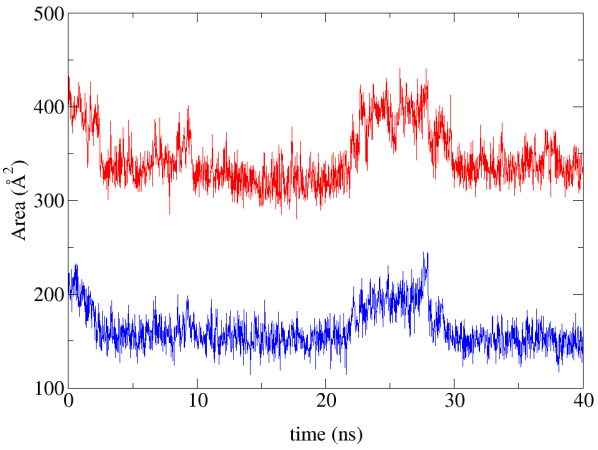

Figure S28. SASA of **4**-β-CD components.

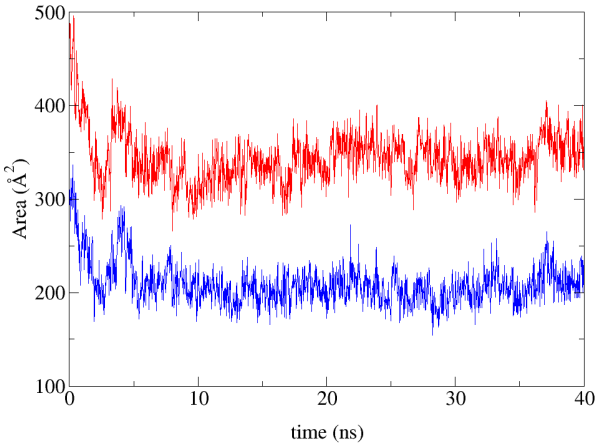

Figure S29. SASA of **4**-γ-CD components.

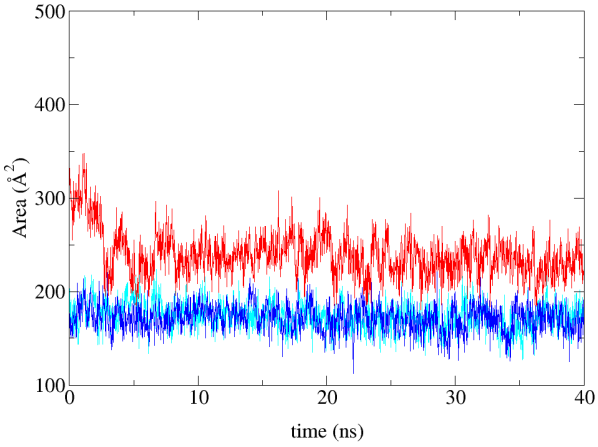

Figure S30. SASA of **4**-2β-CD (antiparallel) components.

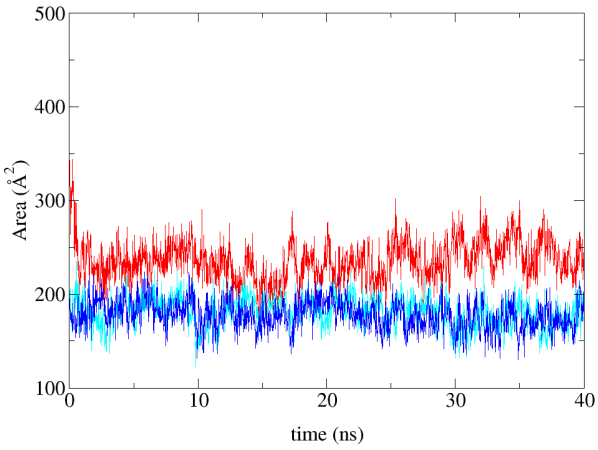

Figure S31. SASA of **4**-2β-CD (parallel) components.

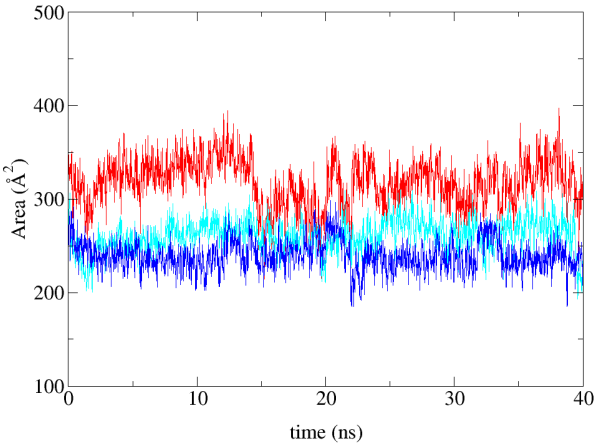

Figure S32. SASA of **4**-2γ-CD (antiparallel) components.

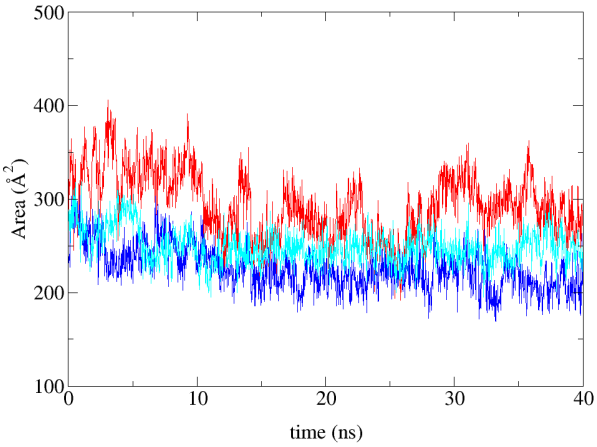

Figure S33. SASA of **4**-2γ-CD (parallel) components.

F. Asymmetry between cyclodextrins

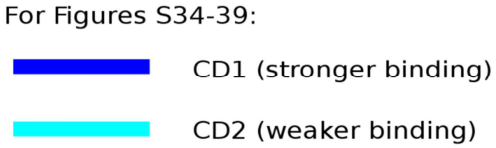

Legend for figures S34-39.

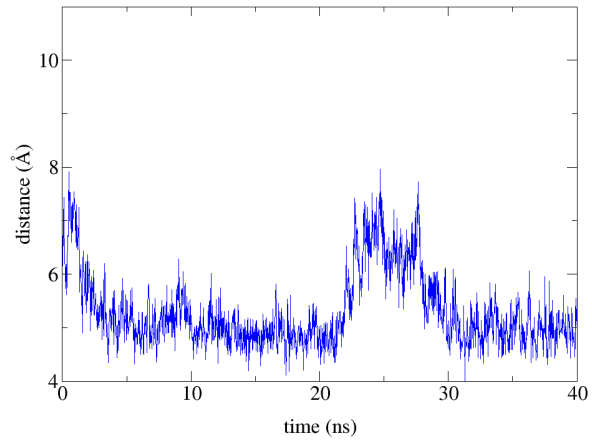

Figure S34. Mass-weighed distance between CD and **4** in **4**-β-CD.

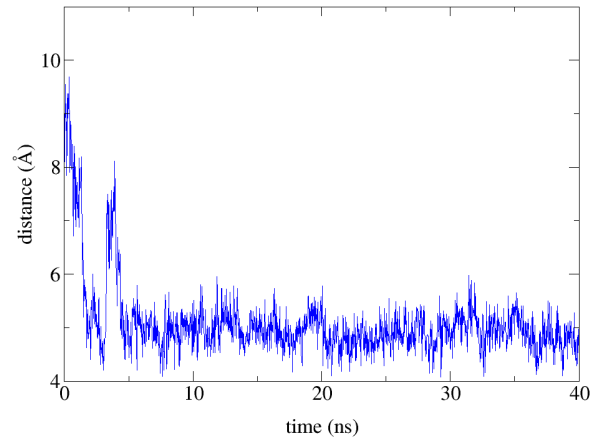

Figure S35. Mass-weighed distance between CD and **4** in **4**-γ-CD.

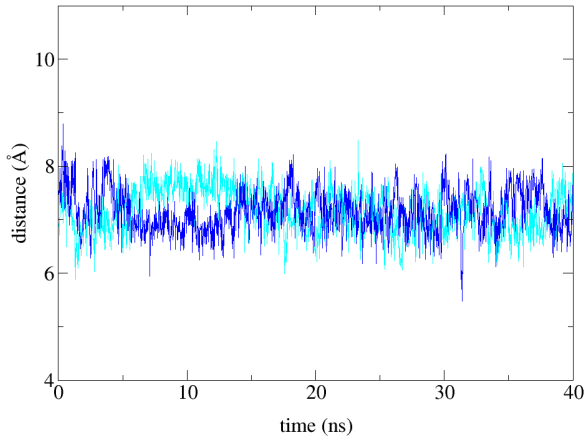

Figure S36. Mass-weighed distance between CDs and **4** in **4**-2β-CD (antiparallel).

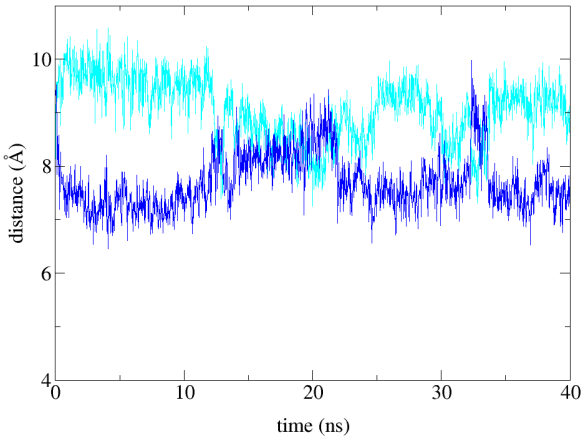

Figure S37. Mass-weighed distance between CDs and **4** in **4**-*2γ-CD* (antiparallel).

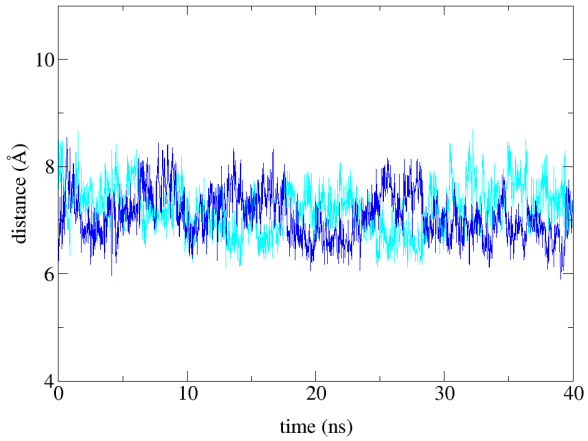

Figure S38. Mass-weighed distance between CDs and **4** in **4**-*2β-CD* (parallel).

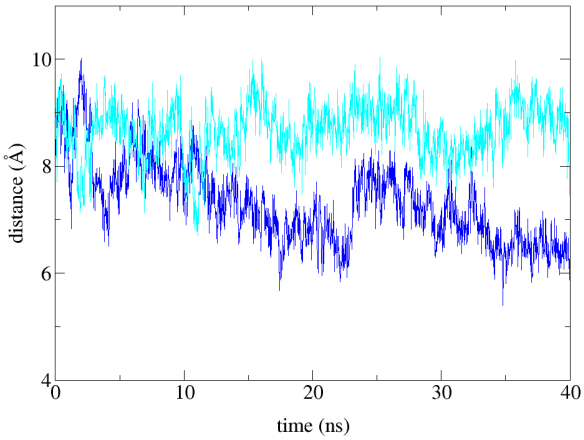

Figure S39. Mass-weighed distance between CDs and **4** in **4**-2γ-CD (parallel).

G. Shape of macrocycle 4

While cyclodextrin molecules generally do not change their shape upon binding, **4** is a relatively flexible molecule. To check the influence of catenane formation on the shape of macrocycle **4**, we measured the distance between the centers of masses of opposite S-S bonds. While **4** alone is folded into a highly elongated shape, it turns into a bent rhombus upon cyclodextrin binding and for antiparallel **4**-2β-CD the azobenzenes form almost a square shape.

For Figures S40-46:

SS-SS distance (long axis)

SS-SS distance (short axis)

Legend for figures S40-46.

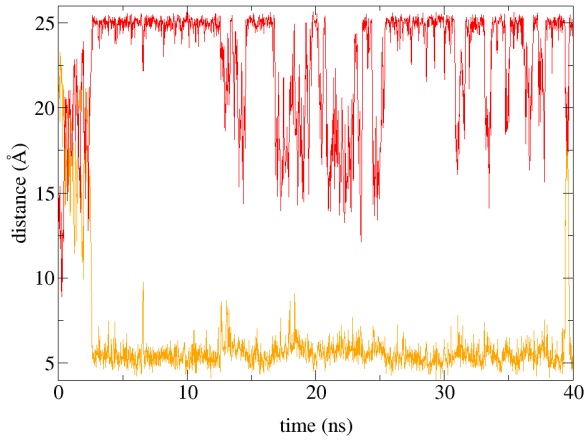

Figure S40. Distances between opposite disulfide bonds in **4**.

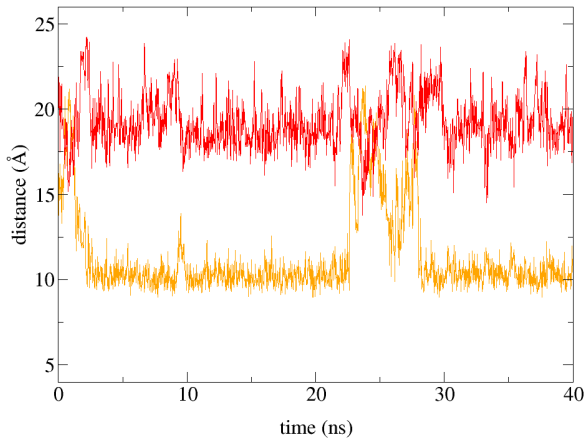

Figure S41. Distances between opposite disulfide bonds in **4**-β-CD.

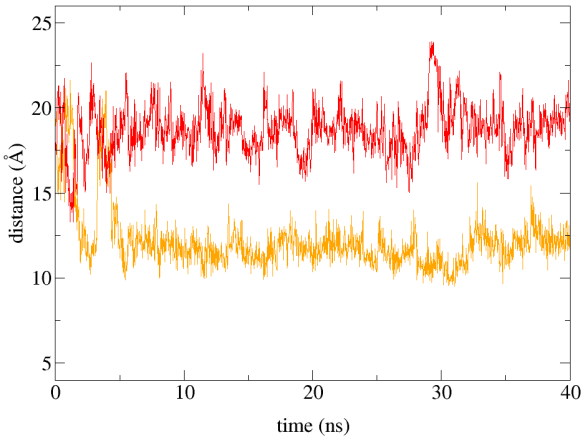

Figure S42. Distances between opposite disulfide bonds in **4**-γ-CD.

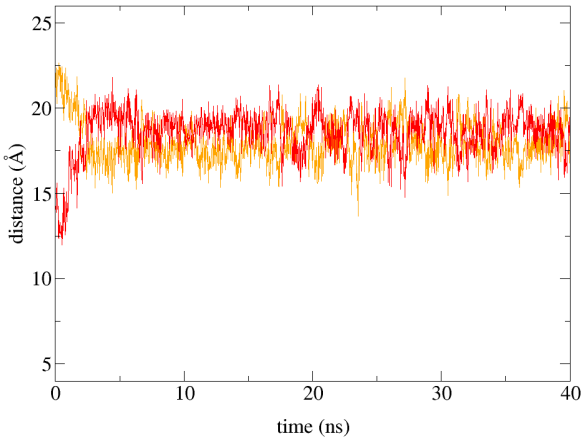

Figure S43. Distances between opposite disulfide bonds in **4**-2β-CD (antiparallel).

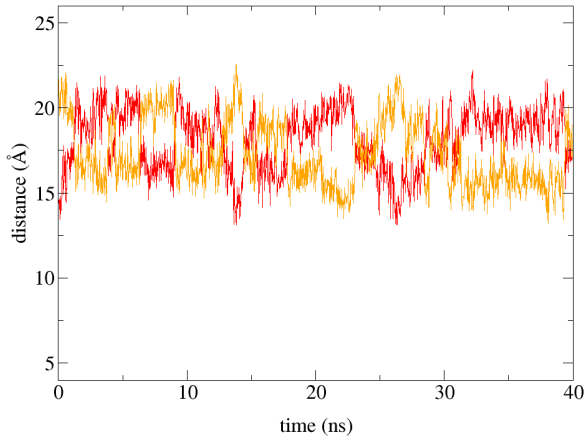

Figure S44. Distances between opposite disulfide bonds in 4-2β-CD (parallel).

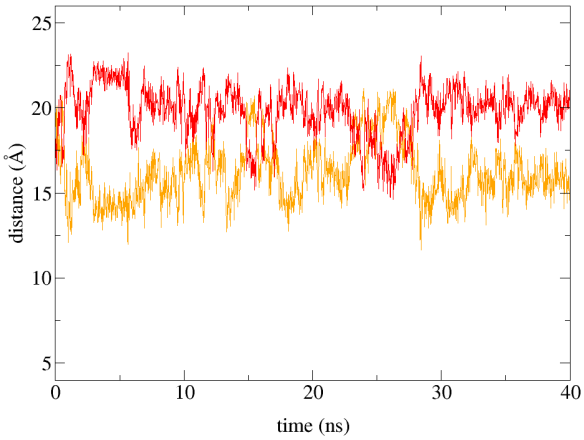

Figure S46. Distances between opposite disulfide bonds in **4**-2γ-CD (parallel).

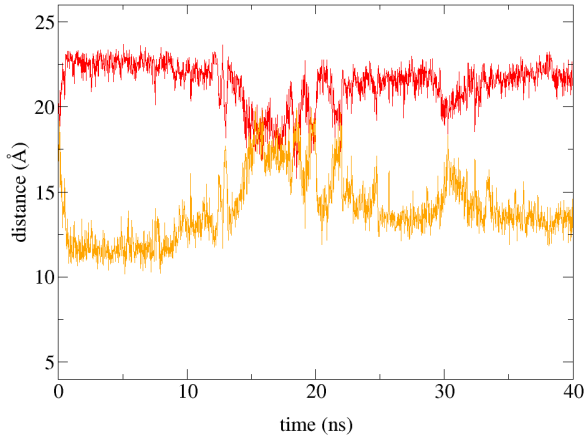

Figure S45. Distances between opposite disulfide bonds in **4**-2γ-CD (antiparallel).

H. Hydrogen bonding interactions between 4 and the cyclodextrins

Table S5. Intermolecular hydrogen bonds between CDs and 4, averaged over last 20 ns of simulations

	4-β-CD	**4**-γ-CD	**4**-2β-CDa	**4**-2β-CDp	**4**-2γ-CDa	**4**-2γ-CDp
CD1	3.6±0.2	4.2±0.4	3.1±0.1	3.2±0.3	3.8±0.2	3.6±0.7
CD2			3.1±0.3	3.6±0.2	3.6±0.5	3.3±0.6

8. HPLC Analysis of DCLs Without/With α-CD

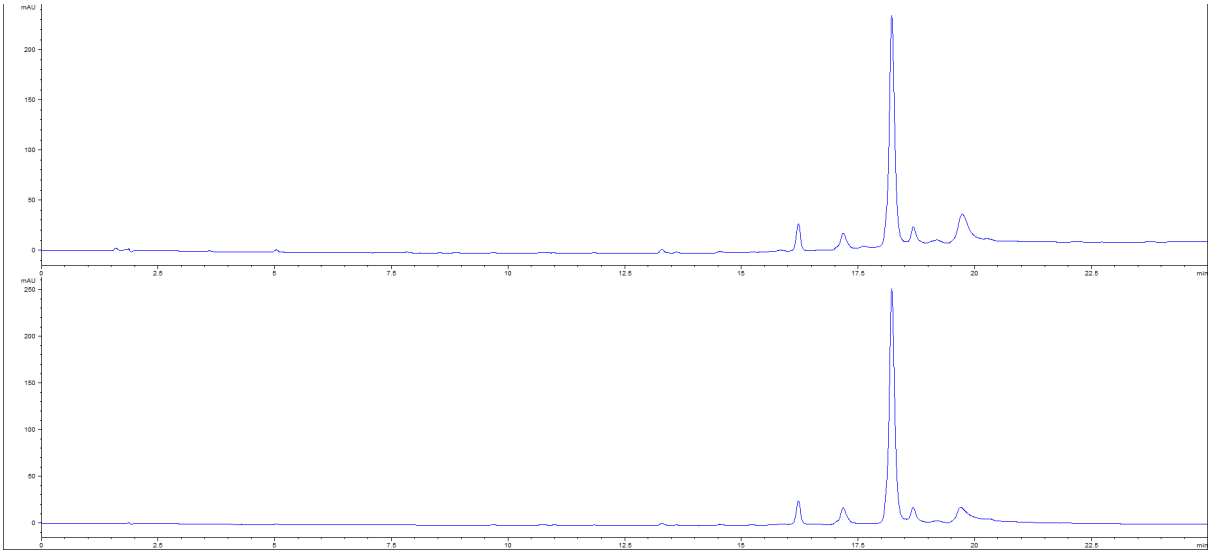

Figure S46. HPLC analysis of libraries made from 2.0 mM building block **1** in aqueous borate buffer (50 mM, pH 8.2) (a) without α-CD; (b) with 4.0 eq. α-CD.

9. References

(1) Benesi, H. A.; Hildebrand, J. H. *J. Am. Chem. Soc.* **1949**, *71*, 2703-2707.

(2) Kuntz, I. D.; Gasparro, F. P.; Johnston, M. D.; Taylor, R. P. *J. Am. Chem. Soc.* **1968**, *90*, 4778-4781.

(3) K. N. Kirschner and R. J. Woods, *Proc. Natl. Acad. Sci. U. S. A.*, **2001**, *98*, 10541.

(4) M. Basma, S. Sundara, D. Calgan, T. Venali and R. J. Woods, *J. Comput. Chem.*, **2001**, *22*, 1125.

(5) K. N. Kirschner and R. J. Woods, *J. Phys. Chem. A*, **2001**, *105*, 4150.

(6) Cézard, C.; Trivelli, X.; Aubry, F.; Djedaïni-Pilard, F.; Dupradeau, F.-Y., *Phys. Chem. Chem. Phys.*, **2011**, 13, 15103–21.

(7) J. Wang, R. M. Wolf, J. W. Caldwell, P. A. Kollman and D. A. Case, *J. Comput. Chem.*, **2004**, *25*, 1157-1174.

(8) Duchstein, P.; Neiss, C.; Görling, A.; Zahn, D., *J. Mol. Model.*, **2012**, 18, 2479–82.

(9) F.-Y. Dupradeau, A. Pigache, T. Zaffran, C. Savineau, R. Lelong, N. Grivel, D. Lelong, W. Rosanski, P. Cieplak, *Phys. Chem. Chem. Phys.*, **2010**, 12, 7821-7839.

(10) Gaussian 09, Revision C.01, M. J. Frisch, G. W. Trucks, H. B. Schlegel, G. E. Scuseria, M. A. Robb, J. R. Cheeseman, G. Scalmani, V. Barone, B. Mennucci, G. A. Petersson, H. Nakatsuji, M. Caricato, X. Li, H. P. Hratchian, A. F. Izmaylov, J. Bloino, G. Zheng, J. L. Sonnenberg, M. Hada, M. Ehara, K. Toyota, R. Fukuda, J. Hasegawa, M. Ishida, T. Nakajima, Y. Honda, O. Kitao, H. Nakai, T. Vreven, J. A. Montgomery, Jr., J. E. Peralta, F. Ogliaro, M. Bearpark, J. J. Heyd, E. Brothers, K. N. Kudin, V. N. Staroverov, T. Keith, R. Kobayashi, J. Normand, K. Raghavachari, A. Rendell, J. C. Burant, S. S. Iyengar, J. Tomasi, M. Cossi, N. Rega, J. M. Millam, M. Klene, J. E. Knox, J. B. Cross, V. Bakken, C. Adamo, J. Jaramillo, R. Gomperts, R. E. Stratmann, O. Yazyev, A. J. Austin, R. Cammi, C. Pomelli, J. W. Ochterski, R. L. Martin, K. Morokuma, V. G. Zakrzewski, G. A. Voth, P. Salvador, J. J. Dannenberg, S. Dapprich, A. D. Daniels, O. Farkas, J. B. Foresman, J. V. Ortiz, J. Cioslowski, and D. J. Fox, Gaussian, Inc., Wallingford CT, **2010**.

(11) M. D. Hanwel, D.E. Curtis, D.C. Lonie, T. Vandermeersch, E. Zurek, G. R. Hutchison., *J. Cheminform.*, **2012**, *4*, 17.

(12) D.A. Case, T.A. Darden, T.E. Cheatham, III, C.L. Simmerling, J. Wang, R.E. Duke, R. Luo, R.C. Walker, W. Zhang, K.M. Merz, B. Roberts, S. Hayik, A. Roitberg, G. Seabra, J. Swails, A.W. Götz, I. Kolossváry, K.F. Wong, F. Paesani, J. Vanicek, R.M. Wolf, J. Liu, X. Wu, S.R. Brozell, T. Steinbrecher, H. Gohlke, Q. Cai, X. Ye, J. Wang, M.-J. Hsieh, G. Cui, D.R. Roe, D.H. Mathews, M.G. Seetin, R. Salomon-Ferrer, C. Sagui, V. Babin, T. Luchko, S. Gusarov, A. Kovalenko, and P.A. Kollman (**2012**), AMBER 13, University of California, San Francisco.

(13) W. L. Jorgensen, J. Chandrasekhar, J. D. Madura, R. W. Impey, M. L. Klein, *J. Chem. Phys*., **1983**, *79*, 926-935.

(14) J. P. Ryckaert, G. Ciccotti, H. J. C. Berendsen, *JCoPh*, **1977**, *23*, 327-341.

(15) J. A. Izaguirre, D. P. Catarello, J. M. Wozniak, R. D. Skeel, *J. Chem. Phys*., **2001**, *114*, 2090-2098

(16) H. J. C. Berendsen, J. P. M. Postma, W. F. Vangunsteren, A. Dinola, J. R. Haak, *J. Chem. Phys.*, **1984**, *81*, 3684-3690.

(17) T. Darden, D. York, L. Pedersen, *J. Chem. Phys*., **1993**, *98*, 10089-10092

(18) D.A. Case, T.A. Darden, T.E. Cheatham, III, C.L. Simmerling, J. Wang, R.E. Duke, R. Luo, R.C. Walker, W. Zhang, K.M. Merz, B. Roberts, B. Wang, S. Hayik, A. Roitberg, G. Seabra, I. Kolossváry, K.F. Wong, F. Paesani, J. Vanicek, J. Liu, X. Wu, S.R. Brozell, T. Steinbrecher, H. Gohlke, Q. Cai, X. Ye, J. Wang, M.-J. Hsieh, G. Cui, D.R. Roe, D.H. Mathews, M.G. Seetin, C. Sagui, V. Babin, T. Luchko, S. Gusarov, A. Kovalenko, and P.A. Kollman (**2010**), AMBER 11, University of California, San Francisco.

(19) W. Humphrey, A. Dalke, K. Schulten, *J. Molec. Graphics*, **1996**, *14*, 33-38, http://www.ks.uiuc.edu/Research/vmd/

(20) Nowak, P.; Li, J.; Fanlo Virgos, H.; Otto, S. *figshare* Retrieved 14:41, Jan 09, 2014 (GMT) http://dx.doi.org/10.6084/m9.figshare.897966

(21) W. Noordman, W. Blokzijl, J. Jager, J. B. F. N. Engberts and M.J. Blandamer., *J. Org. Chem*., **1993**, *58*, 7111-7114.

(22) P. Hol, L. Streefland, M.J. Blandamer and J. B. F. N. Engberts., *J. Chem. Soc., Perkin Trans. 2*, **1997** 485-488.